Automatic Registration of Vestibular Systems with Exact Landmark Correspondence

Minqi Zhang[e], Fang Li[e], Xingce Wang[f], Zhongke Wu[f], Shi-Qing Xin[g], Lok-Ming Lui[h], Ying He[e]

[e] *School of Computer Engineering, Nanyang Technological University, Singapore*
[f] *College of information science and technology, Beijing Normal University, Beijing, China*
[g] *Faculty of Information Science and Engineering, Ningbo University, Zhejiang, China*
[h] *Department of Mathematics, Chinese University of Hong Kong, Hong Kong, China*

Abstract

Shape registration has a wide range of applications in geometric modeling, medical imaging, and computer vision. This paper focuses on the registration of the genus-3 vestibular systems and studies the geometric differences between the normal and Adolescent Idiopathic Scoliosis (AIS) groups. The non-trivial topology of the VS poses great technical challenges to the geometric analysis. To tackle these challenges, we present an effective and practical solution to register the vestibular systems. We first extract six geodesic landmarks for the VS, which are stable, intrinsic, and insensitive to the VS's resolution and tessellation. Moreover, they are highly consistent regardless of the AIS and normal groups. The detected geodesic landmarks partition the VS into three patches, a topological annulus and two topological disks. For each pair of patches of the AIS subject and the control, we compute a bijective map using the holomorphic 1-form and harmonic map techniques. With a carefully designed boundary condition, the three individual maps can be glued in a seamless manner so that the resulting registration is a homeomorphism with exact landmark matching. Our method is robust, automatic and efficient. It takes only a few seconds on a low-end PC, which significantly outperforms the non-rigid ICP algorithm. We conducted a student's t-test on the test data. Computational results show that using the mean curvature measure E_H, our method can clearly distinguish the AIS subjects and the normal subjects.

Keywords: registration, landmark matching, vestibular system, discrete geodesic, harmonic map, holomorphic 1-form

1. Introduction

Surface registration is the process that aligns a source 3D surface to a target. It has a wide range of applications in geometric modeling, medical imaging, and computer vision. This paper focuses on registration of the vestibular systems (VS) and studies the geometric differences between the normal and Adolescent Idiopathic Scoliosis (AIS) groups. The vestibular system is the sensory system situated in the inner ear, which contributes to balance and the sense of spatial orientation. The VS is a genus-3 structure with three semicircular canals (see Figure 1(a)) and the morphometry of VS plays an important role in the analysis of various diseases such as the AIS disease, which is a 3D spinal deformity affecting about 4% school children worldwide. The etiology of AIS is still unclear but believed to be a multi-factorial disease. One popular hypothesis was suggested to be the structural changes in the VS that induce the disturbed balance perception, and further cause the spinal deformity [1, 2]. Some recent works have revealed the statistical differences in global morphology of the VS between right-thoracic AIS and normal controls [3, 4]. In order to perform shape analysis effectively, meaningful one-to-one correspondence between different VSs must be obtained. Landmark-matching based registration techniques, in which landmark features were required to be consistently matched to guide the registration, have proven to be effective in obtaining accurate point-wise correspondences between 3D medical data. However, the non-trivial topology of the VS poses great challenges for the landmark based registration. The existing surface registration algorithms either work only for shapes with simple topology (e.g., simply or multiply connected domains) or are too time consuming and memory inefficient, which are not suitable for our problem.

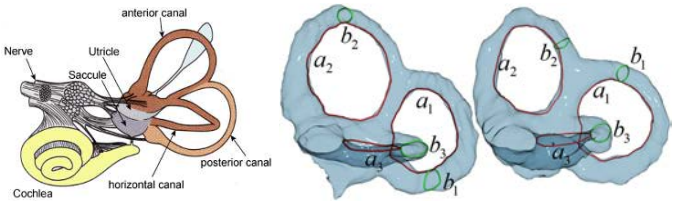

(a) The labyrinth of the inner ear (courtesy of wikipedia)

(b) The homology basis of the genus-3 VS

Figure 1: The vestibular system is a genus-3 structure (colored in brown) in the inner ear. Its homology basis $\{a_i, b_i\}_{i=1}^{3}$ of the genus-3 vestibular system contains 6 loops. Among them, the three geodesic *tunnel* loops a_i are highly consistent regardless of the AIS/normal subjects. The locations of the geodesic *handle* loops b_i, however, may vary significantly.

This paper presents a computational framework to register the vestibular systems. Our contributions are two-folded:

Email addresses: mzhang1@e.ntu.edu.sg (Minqi Zhang), asfli@ntu.edu.sg (Fang Li), wangxingce@bnu.edu.cn (Xingce Wang), zwu@bnu.edu.cn (Zhongke Wu), xinshiqing@nbu.edu.cn (Shi-Qing Xin), lmlui@math.cuhk.edu.hk (Lok-Ming Lui), yhe@ntu.edu.sg (Ying He)

- First, we present a robust algorithm to extract the salient geodesic landmark features from the vestibular systems. Thanks to its intrinsic nature, the geodesic landmarks are totally determined by the metric and are highly consistent regardless of the AIS and normal groups.

- Second, we present an efficient algorithm to register the vestibular systems with exact landmark correspondence. We first partition each VS into three patches, a topological annulus and two topological disks, using the extracted landmark features. Then for each pair of patches of the AIS subject and the control, we compute a bijective map using the holomorphic 1-form and harmonic map techniques. With a carefully designed boundary condition, the three individual maps can be glued in a seamless manner. The resulting registration is guaranteed to be a homeomorphism with exact landmark correspondence.

To our knowledge, this is the first work to address the landmark based registration of the vestibular systems. Our method is robust, automatic and efficient, which takes only a few seconds on a low-end PC. We have tested our algorithms on 13 normal subjects and 15 AIS patients. Computational results show that our method can distinguish the AIS subjects and normal subjects by using the mean curvature measure.

2. Related Work

As a fundamental problem in medical imaging, digital geometry processing and graphics, surface registration has been studied extensively in the past two decades. Most of the existing registration algorithms focus on rigid registration, where the motion between the source and the target is rigid. Representative work is the iterative closest point (ICP) algorithm [5], which iteratively computes correspondence between the source and the target, and performs a rigid motion in response to these correspondences. Rigid registration and non-rigid registration under small deformation are ideal for 3D scanning systems, in which the source and the target are the overlapped scans of static model. However, they are not suitable for our problem, where the deformation between the source and the target could be large.

Recently, non-rigid registration dealing with large deformation has attracted increasing attention. Huang et al. [6] formulated non-rigid registration as an optimization problem and solved it by alternating correspondence computation and deformation optimization in terms of the resulting correspondences. By enforcing the geodesic distances between sets of corresponding points, their method is highly stable and works well for aligning partially overlapping point clouds, which are sampled from models under isometric deformation. However, the mapping between two VS surfaces are in general not isometric, their method cannot be applied to our problem.

Amberg et al. [7] proposed the optimal step non-rigid ICP algorithm, which recovers global and local deformations of the mesh by successive application of ICP. Starting with a stiff template, the algorithm successively relaxes the stiffness to recover more local deformations. To find the optimal deformation for a given stiffness, optimal iterative closest point steps are used. Their method can handle missing data robustly and is also insensitive to initial conditions. However, their method is memory inefficient and time consuming.

Salzmann et al. [8] focused on 3D shape recovery of deformable surfaces from individual images. Unlike the other approaches that require initial shape estimates and track deformations from image to image, their method produces the non-rigid registration in a closed-form solution. Their method assumes the to-be-recovered shape is of rectangular shape (i.e., a topological disk) under isometric deformation, therefore, it cannot work for the VS due to its non-trivial topology and non-isometric deformation.

The large deformation diffeomorphic metric mapping (LDDMM) framework [9, 10, 11] places the shapes in a metric space, and provides a diffeomorphic transformation by solving the transport equation of a time dependent vector field. The LDDMM framework is theoretically sound and elegant, which can guarantee a diffeomorphism with exact landmark matching. However, the high computational cost and memory requirement diminish its application to large surfaces.

The above-mentioned registration methods are extrinsic in the sense they align the source to the target via computing the transformation in the embedding space $\mathbb{R}^3$. In contrast, the parameterization based methods find the mapping between the source and the target in an intrinsic manner. Conformal maps [12, 13] have received increasing attention due to their smooth and angle preserving features. Zeng et al. [14] tackled the non-rigid registration problem using slit map, where the source and the target are multiply connected domains (i.e., genus-0 surface with $n(\geq 2)$ boundaries). Each surface is conformally mapped to a rectangular domain with $n-2$ horizontal slits. Then they computed a harmonic map between two rectangular domains such that the boundaries and slits are mapped to each other. Their method solves only a few sparse linear system, therefore, it is very efficient. However, the topology constraint diminishes its applications to only multiply connected domains. Furthermore, conformal maps do not allow for boundary positions to be prescribed. As a result, landmarks cannot be exactly matched and bijectivity cannot be ensured when large number of landmark constraints are enforced.

The space of quasi-conformal map [15, 16] naturally extends the space of conformal maps by allowing bounded angle distortion. Among all quasi-conformal maps, the extremal quasi-conformal map [17][18] is of particular interest, due to its many promising features, such as uniqueness, minimizing the maximal angle distortion, and allowing for solution of boundary value problems. Unfortunately, only techniques for computing the extremal quasi-conformal maps on planar domain or 3D surfaces of simple topology (i.e., genus zero or one) are available. Computing such maps for 3D surfaces with genus $g \geq 2$ (as required in our application), however, is non-trivial.

Table 1 lists the features of the major non-rigid surface registration methods. Most of the existing methods either work only for models with simple topology or do not support landmark matching. The LDDMM algorithm [9] and the optimal

Method	Application domain	Landmark matching	Map quality	Computational cost
Huang et al. [6]	3D surfaces under isometric deformation	no	isometric transformation	high
LDDMM [9]	2D/3D grids	yes	diffeomorphism	high
Extremal quasi-conformal map [17]	simply/multiply connected domain, genus-0 or 1 surfaces	yes	diffeomorphism	low
Holomorphic differentials [14]	multiply connected domain	yes	diffeomorphism	low
Salzmann et al. [8]	simply connected domain	yes	homeomorphism	low
Optimal step non-rigid ICP [7]	general 3D surfaces	yes	no guarantee for bijection	high
Our method	genus-3 VS surface	yes	homeomorphism	low

Table 1: Comparison to the existing non-rigid surface registration algorithms.

step non-rigid ICP algorithm [7] are not practical either, due to their extremely high computational costs. Unlike to the existing methods that aim at solving the general non-rigid registration problem, the proposed method is an *ad hoc* solution to the genus-3 VS. It is fully automatic and highly efficient, which takes only a few seconds on a low-end PC. Besides, it guarantees the exact landmark matching and bijectivity, which makes it a practical solution to our problem.

3. Algorithm

Our framework contains two stages, the first stage is to detect the landmarks using stable geodesic loops and the second one is to parameterize the VS surface using holomorphic 1-form and harmonic maps. Our registration method can guarantee the bijection and the exact correspondence between the landmarks.

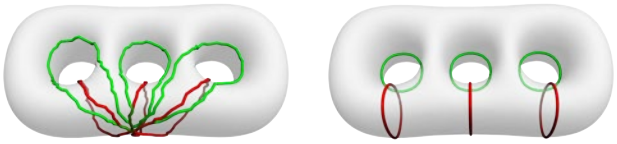

(a) System of loops (b) Homology basis

Figure 2: Computing the geodesic homology basis on the 3-torus model.

3.1. Landmark Extraction

Let us denote S the boundary surface of the vestibular system, which is a closed oriented 3D surface of genus $g = 3$. S is topologically equivalent to a sphere with three handles, which are horizontal canal, anterior canal, and posterior canal, denoted by γ_1, γ_2 and γ_3 respectively. The horizontal canal γ_1, is roughly orthogonal to the other two regardless of the normal/AIS groups, see Figure 1(a).

It is well known that one can cut a genus g surface S into a topological disk by $2g$ loops, which form the basis of the homology group. Dey et al. [19] defined two classes of loops, called tunnel and handle loops in terms of a homology group. A loop is a *tunnel* (resp. *handle*) if it spans a surface, say D, in the *unbounded* (resp. *bounded*) space bordered by S and does not do so in S. Intuitively speaking, if one cuts S along a tunnel loop and fills the boundaries with two copies of D, one eliminates a handle. Similarly, removing a handle loop eliminates a tunnel. See Figure 2.

Xin et al. observed that the geodesic tunnels on the VS surface can be used to study the geometric differences between the normal and AIS groups [4]. In this paper, we adopt Xin et al.'s approach [4] to compute the three geodesic tunnels a_1, a_2 and a_3 (see the red curves in Figure 1). As a byproduct, Xin et al.'s algorithm also produces the dual *geodesic* loops b_i, $i = 1, 2, 3$. Together $\{a_i, b_i\}_{i=1}^3$ form the homology basis of the genus-3 VS, such that the intersection numbers of the paths are $a_i \cdot a_j = b_i \cdot b_j = 0$ and $a_i \cdot b_j = \delta_{ij}$.

It is worth noting that the geodesic tunnel loops a_i, $i = 1, 2, 3$, are highly stable, regardless of the AIS and normal groups. However, the locations of the dual loops b_i may vary significantly (see Figure 1(b)). To obtain consistent landmark features, we adopt the following strategy: for each pair of handles, say γ_i and γ_j, we find a pair of points $p_i \in b_i$ and $p_j \in b_j$. Then we use Dijkstra's algorithm to find a path l_{ij} connecting p_i and p_j. The path $c_{ij} \triangleq b_i l_{ij} b_j l_{ij}^{-1}$ is homotopic to $b_i + b_j$. Next, we apply Xin et al.'s curve shortening algorithm [20] to deform c_{ij} into a geodesic loop (see Figure 3). As Xin et al.'s algorithm keeps the curve's topology during the length shortening process, c_{ij} is homotopic to $b_i + b_j$. Furthermore, as geodesic is intrinsic and geometry aware, the computed loop c_{ij} is insensitive to the initial curve $b_i l_{ij} b_j l_{ij}^{-1}$. We observe the geodesic loops a_i, c_{ij} are highly consistent among AIS/normal subjects, thus, can be used as the landmark features (see Figure 4). The pseudocode of landmark extraction is shown in Algorithm 1.

Input: A vestibular system (VS) surface S
Output: Six geodesic landmark features
1. Compute the geodesic homology basis $\{a_i, b_i\}$ for each handle γ_i, $i = 1, 2, 3$.
2. For any two handles γ_i and γ_j,
3. Choose two arbitrary points $p_i \in b_i$ and $p_j \in b_j$.
4. Find a path l_{ij} connecting p_i and p_j using Dijkstra's shortest path algorithm.
5. Deform $b_i l_{ij} b_j l_{ij}^{-1}$ into a geodesic loop c_{ij} using [20].
6. End For
7. Output $\{a_1, a_2, a_3, c_{12}, c_{23}, c_{31}\}$.

Algorithm 1: Extracting the six geodesic landmarks from a VS surface.

The extracted geodesic landmarks naturally induce a surface segmentation: cutting S along the geodesic loops c_{12}, c_{23} and c_{31} produces a genus-1 surface with three boundaries and a genus-0 surface with three boundaries. Further cutting the two

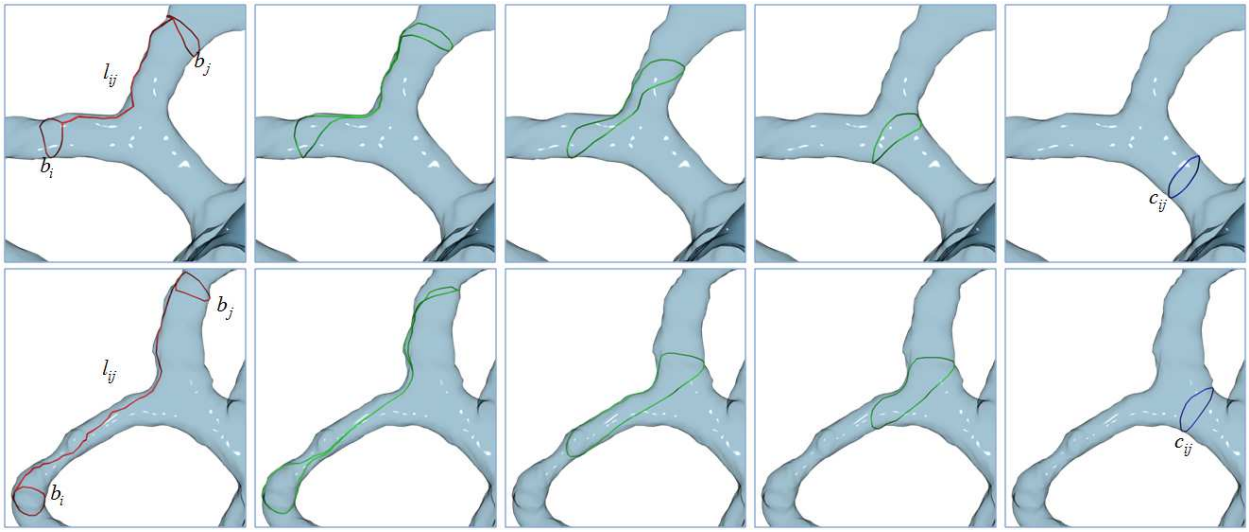

Figure 3: Computing the stable geodesic loop c_{ij} across two handles γ_i and γ_j. From left to right: the initial curve $b_i l_{ij} b_j l_{ij}^{-1}$ (in red) is continuously deformed into a stable geodesic loop c_{ij} (in blue). The intermediate loops are rendered in green. Note that the final geodesic loop is homotopic to the initial curve, since the curve shortening method [20] keeps the curve's topology during the deformation.

surfaces along the geodesic *tunnel* loops a_1, a_2 and a_3, we obtain three patches, i.e., a topological annulus P_1 and two topological disks P_2 and P_3 (see Figure 5). The six feature points, $a_1 \cap c_{12}$, $a_1 \cap c_{31}$, $a_2 \cap c_{12}$, $a_2 \cap c_{23}$, $a_3 \cap c_{23}$, $a_3 \cap c_{31}$, are defined as the intersection of two landmark curves. Note that each boundary ∂P_i, $i = 1, 2, 3$, has exactly 6 feature points, which allows us to define a boundary condition in the registration so that the landmark curves can be matched.

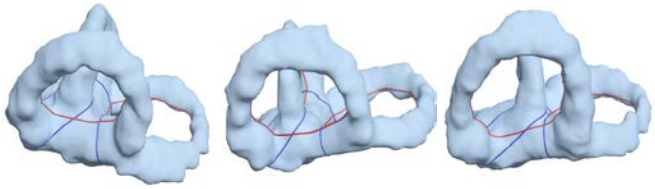

(a) Normal subjects

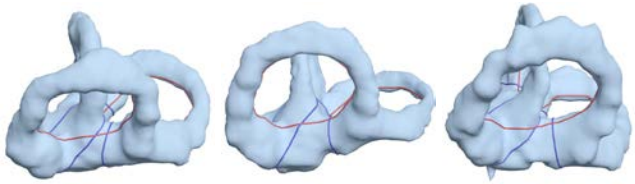

(b) AIS subjects

Figure 4: Thanks to the intrinsic and geometry-aware nature of the geodesic loops, the extracted landmarks are stable and highly consistent among the AIS and normal subjects.

3.2. Registration

Given two VS surfaces S^1 and S^2 with the extracted landmarks $\{a_1^i, a_2^i, a_3^i, c_{12}^i, c_{23}^i, c_{31}^i\}$, $i = 1, 2$, our goal is to find a bijective map $\phi : S^1 \to S^2$ with exact landmark correspondence, i.e., $\phi(a_1^1) = a_1^2$, $\phi(c_{12}^1) = c_{12}^2$, etc. As each VS surface can be segmented into three genus-0 patches, $S^i = \bigcup_{j=1}^3 P_j^i$, $i = 1, 2$, our idea is to find a bijective map $\phi_i : P_i^1 \to P_i^2$ between each pair of patches. With a carefully designed boundary condition for each individual map, we can "glue" them together to form the bijective map with exact landmark correspondence. See Algorithm 2 for the pseudocode of the registration algorithm.

3.2.1. Computing the map between two topological annuli

The patch P_1 containing three semicircular canals is the major component of the VS. Its geometry resembles a long tube and its topology is equivalent to an annulus. We first parameterize the patch P_1 to a canonical annulus (with outer radius equals 1) using the Gu-Yau method [21]. Then we cut the annulus open and map it to a rectangle using the complex logarithm function $z \mapsto \log z$. Let t denote the conformal map from the patch P_1 to the annulus and g denote the conformal map from the annulus to a rectangle. Then the composite map $g \circ t$ maps P_1 to a rectangular domain R.

Now given two patches P_1^1 and P_1^2, we compute the maps $g_1 \circ t_1 : P_1^1 \to R_1$ and $g_2 \circ t_2 : P_1^2 \to R_2$. Then we compute a harmonic map $r : R_1 \to R_2$ between the two rectangles. Similar to the harmonic function d in the disk map, we specify the Dirichlet boundary condition by matching the feature points and parameterize the non-feature points using arc length parameterization. Finally, the annulus map $\phi_1 : P_1^1 \to P_1^2$ is defined as $\phi_1 = t_2^{-1} \circ g_2^{-1} \circ r \circ g_1 \circ t_1$, See the commutative diagram in Figure 6(a).

3.2.2. Computing the map between two topological disks

Observe that both P_2 and P_3 are topological disks and the boundary of each disk has 6 feature points, which are the intersection points of landmark curves. Here we present the method to compute the map $\phi_2 : P_2^1 \to P_2^2$. The other map $\phi_3 : P_3^1 \to P_3^2$ can be constructed in the same way. Let q_j^i, $j = 1, \cdots, 6$ denote the six feature points on ∂P_2^i. We map each disk P_2^i to the unit disk $\mathbb{D}$ by computing a harmonic function $f_i : P_2^i \to \mathbb{D}$, $\Delta f_i = 0$. The Dirichlet boundary condition is specified by using the arc

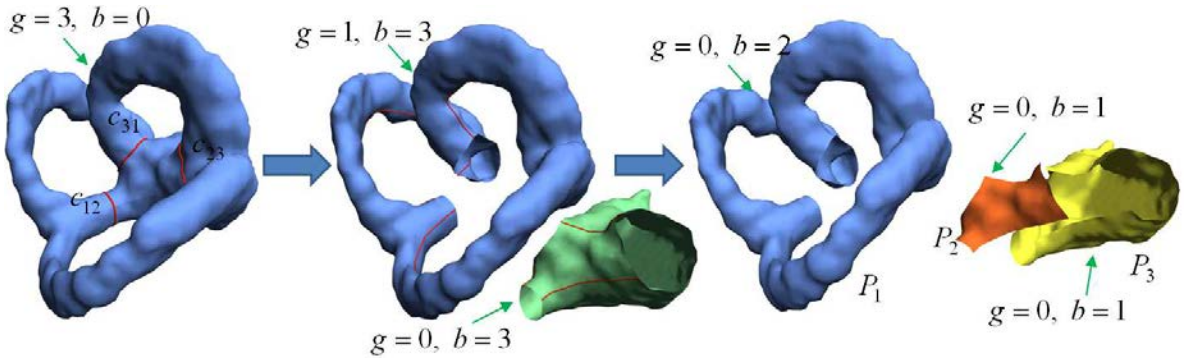

Figure 5: Cutting the VS surface along the geodesic landmarks we obtain 3 genus-0 patches. g: genus, b: number of boundaries.

length parameterization: set the feature point q_1^i as the reference point with $f_i(q_1^i) = e^{\mathbf{i}0}$. Then for any boundary point $q \in \partial D^i$, $f_i(q) = e^{\mathbf{i}\theta(q)}$, where $\theta(q) = 2\pi l(q, q_1^i)/L$, and $l(s,t)$ measures the boundary length from s to t, and L is the total length of the boundary ∂D^i. Next, we compute another harmonic map $d : \mathbb{D} \to \mathbb{D}$, which aligns two unit disks such that the images of the feature points $d(f_1(q_i^2)) = f_2(q_i^2)$ are matched and the non-feature boundary points are determined by the arc-length parameterization. Finally, the map $\phi_2 : P_2^1 \to P_2^2$ is constructed by the composite map $\phi_2 = f_2^{-1} \circ d \circ f_1$. See Figure 6(a) for the commutative diagram.

3.2.3. Constructing the global map

The global map $\phi : S^1 \to S^2$ is simply constructed by gluing all three individual maps together, i.e., $\phi = \bigcup_{i=1}^3 \phi_i$. Here we show the map ϕ is a homeomorphism with exact landmark correspondence. In the disk maps ϕ_2, ϕ_3 and the annulus map ϕ_1, the harmonic functions f_1, f_2, d and r are all diffeomorphic, since the domains and co-domains are all convex and the Dirichlet boundary conditions are homeomorphisms. The holomorphic 1-form induced mappings t_1, t_2 are conformal and diffeomorphic. The complex log functions g_1 and g_2 are also diffeomorphic when restricting the argument to $[0, 2\pi]$. Thus, all three maps ϕ_1, ϕ_2 and ϕ_3 are diffeomorphic for all the interior points.

Although the maps ϕ_i's are calculated individually, they can be glued seamlessly, since we use the arc-length parameterized boundary condition in computing the harmonic maps. Note that each boundary has exactly 6 feature points, which are guaranteed to be matched as required in the Dirichlet boundary conditions used in the harmonic functions f_1, f_2, d and r. For the non-feature points on the boundary, their images are completely determined by the metric since we parameterize them using the arc-length parameterization. Thus, for two adjacent patches sharing a common boundary, both the feature and non-feature points can be matched exactly, which implies that all the boundary maps are homeomorphic. Putting it altogether, the global map, $\phi = \bigcup_i^3 \phi_i$, is in fact a homeomorphism with exact landmark correspondence.

Input: Two vestibular system surfaces S^1 and S^2
Output: The homeomorphism $\phi : S_1 \to S_2$ with guaranteed landmark correspondence
1. Compute the six geodesic landmarks for each VS surface using Algorithm 1.
2. Cut each VS surface into three genus-0 patches P_1, P_2, and P_3, along the extracted landmark features.
3. Compute the map $\phi_1 : P_1^1 \to P_1^2$ between two topological annuli.
4. Compute the map $\phi_2 : P_2^1 \to P_2^2$ between two topological disks.
5. Compute the map $\phi_3 : P_3^1 \to P_3^2$ between two topological disks.
6. Output the map $\phi = \bigcup_{i=1}^3 \phi_i$.

Algorithm 2: Registration of vestibular system surfaces registration with guaranteed landmark correspondence.

4. Results & Comparisons

4.1. Experimental results

We implemented our algorithm in C++ on a PC with an Intel Core2 Quad CPU 2.83GHz and 16GB RAM. TAUCS[1] is adopted as the linear system solver for the harmonic map and holomorphic 1-form methods.

We tested 28 VS surfaces (15 AIS patients and 13 normal subjects), which were extracted from the MRI. Each VS surface is modeled as a triangle mesh with about 4K vertices. Our method is automatic and efficient: computing the geodesic landmark features takes less than 1 second for each VS surface and registering two VS surfaces takes roughly 6 seconds.

To evaluate the difference of VS between the AIS and normal subjects, we computed the average shape for all 13 normal subjects, which is used as our control model (see Figure 8(a)). Let $f : M \to N$ be the mapping from the control M to a VS subject N. Then we defined the following functionals to measure the difference between M and N based on various types of

[1] http://www.tau.ac.il/~stoledo/taucs/

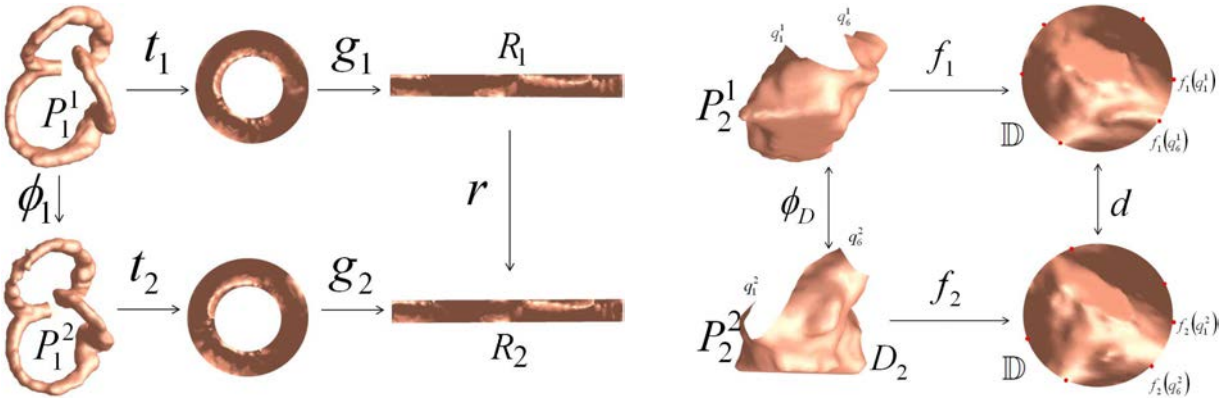

(a) (b)

Figure 6: Registration. (a) The commutative diagram for the map between two topological annuli. (b) The commutative diagram for the map between two topological disks. The red dots are the images of the feature points. To avoid label congestion, only two feature points and their images are labeled, the others can be implied according to the order.

geometric properties,

$$\begin{aligned} E_A &= \int_M |d\sigma - d(\sigma \circ f)|^2 \\ E_K &= \int_M |K - K \circ f|^2 d\sigma \\ E_H &= \int_M |H - H \circ f|^2 d\sigma \\ E_C &= \int_M |\lambda - \lambda \circ f|^2 + s|H - H \circ f|^2 d\sigma \end{aligned}$$

where $\circ$ denotes the function composition, σ is the area element, K is the Gaussian curvature, H is the mean curvature, λ is the conformal factor. The scalar $s > 0$ balances the terms of conformal factor and mean curvature. The functionals E_A, E_K and E_H measure the distortion of area, Gaussian curvature and mean curvature, respectively. The functional E_C extends E_H by considering the conformal factor λ, which measures the stretch distortion of the conformal representation (λ, H). Some results are shown in Figure 10. Figure 9 visualizes the various distortion measures on an AIS subject and a normal subject. Clearly, the AIS subject has larger distortion measures than that of the normal subject.

To verify whether the proposed geometric measures can distinguish the AIS subjects and the normal subjects, we conducted a student's t-test on the 13 normal subjects and 15 AIS subjects. As shown in Figure 7 (row 1), our method produces E_H with a P-value 0.029, which is less than the commonly used threshold 0.05. As a result, the mean curvature difference E_H can be used to distinguish the two groups. Our results also show that the other three measures E_C, E_A and E_K are not statistically important in terms of distinguishing the two groups.

4.2. Comparisons

As discussed in Section 2, most of the existing non-rigid registration algorithms work only for surfaces either under isometric transformations or with simple topology, only the LDDMM algorithm [9] [22] and the optimal step non-rigid ICP algorithm [5] could be used in our problem. In this subsection, we compare our method to these alternative methods.

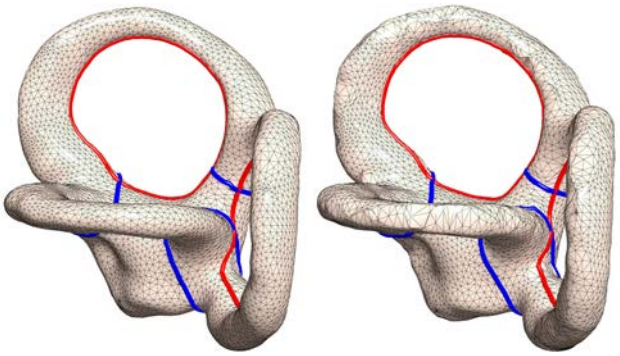

(a) Our result (b) Non-rigid ICP result

Figure 8: Computing the control shape by averaging the 13 normal subjects. Our method guarantees a bijective mapping between any two subjects, whereas the optimal step non-rigid ICP algorithm has no such guarantee. As a result, our result is smoother and has less distortion than that of the ICP algorithm.

The LDDMM algorithm aims to quantify metric distances on anatomical structures in medical images. It is a gradient decent algorithm using the Euler-Lagrange equation to minimize a non-linear energy functional. It guarantees that the computed map is a diffeomorphic and the user-specified landmarks are matched exactly. The LDDMM algorithm can be extended to 3D surfaces by 3-dimensional rasterization (a.k.a. voxelization) so that the velocity field is computed on the voxels. Each iteration takes $O(mn^3)$ time, where m is the number of discretized time intervals, and n is the voxel resolution. In order to obtain an accurate registration, high voxel resolution (i.e., large n) and small time step (i.e., large m) are often desired. Since the LDDMM algorithm is a gradient decent algorithm, it converges very slowly. As a consequence, the LDDMM algorithm is very time consuming and space inefficient. Moreover, implementing the LDDMM algorithm for 3D models with complicated geometry and non-trivial topology is difficult. To our knowledge, only results of models with simple geometry and topology have

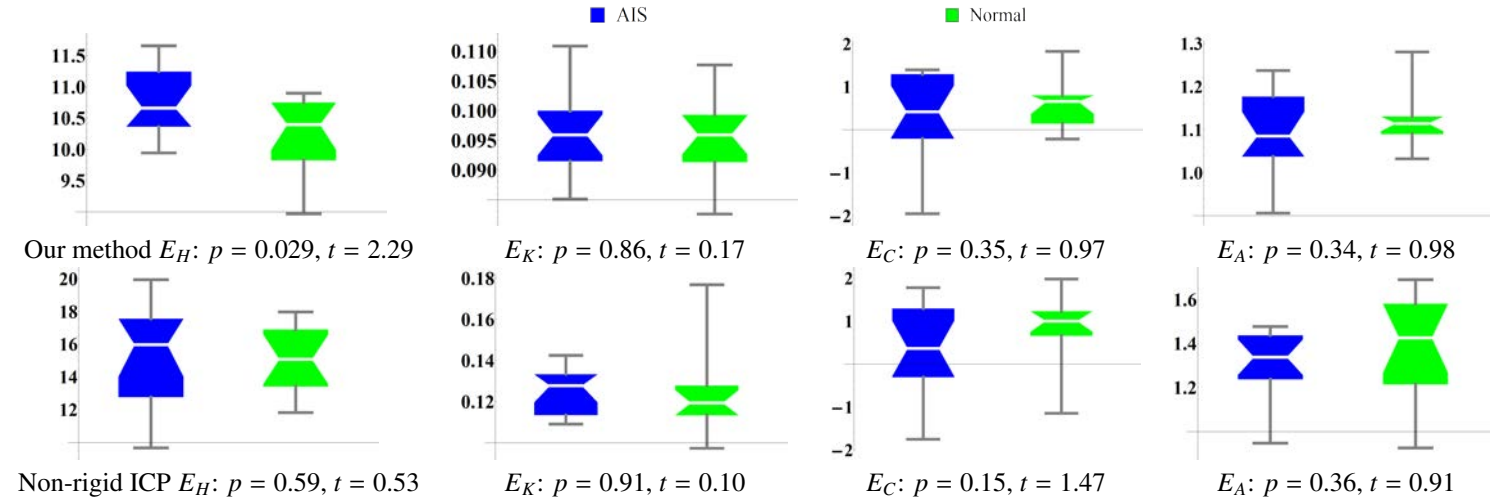

Figure 7: We measure the difference between the AIS subjects and the control model in terms of various geometric features, such as area E_A, Gaussian curvature E_K, mean curvature E_H, and conformal representation E_C. With our method (row 1), the mean curvature difference E_H is statistically significant with a P-value less than 0.05, which implies that we can use mean curvature E_H to distinguish these two groups. Note that the results of the non-rigid ICP method (row 2) are *not* statistically important, since all the resulting P-values are much bigger than the commonly used threshold 0.05.

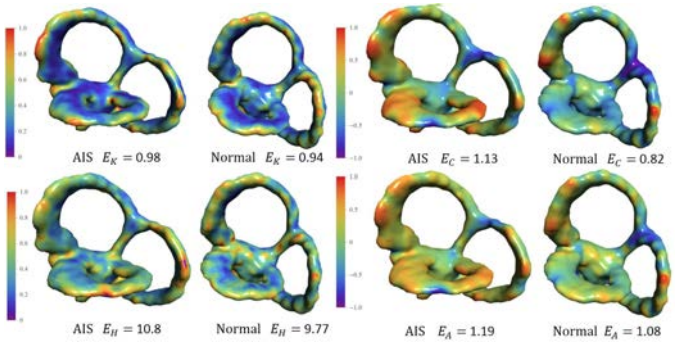

Figure 9: Visualizing the shape distortion measures on an AIS subject and a normal subject. The AIS subjects have larger distortion than the normal subjects.

been reported to date.

The classic ICP algorithm [5] alternates between computing correspondences between the source and target and performing a rigid motion in response to these correspondences. The optimal step non-rigid ICP algorithm [7] extends the ICP algorithm so that it loops over a series of decreasing stiffness weights, and incrementally deforms the template towards the target, recovering the whole range of global and local deformations. The optimal step non-rigid ICP algorithm is extrinsic, since the deformations are carried out in $\mathbb{R}^3$. Their method terminates when all the template vertices are on the target. However, their method cannot guarantee the bijectivity. As shown in Figure 11, when the non-rigid ICP algorithm deforms a smooth template (the control VS) to a target, the part near the features can be easily stuck. Since the nearby vertices are already on the target, the algorithm cannot further improve the mapping. As a result, the deformed shape fails to capture the features. As Figure 10(b) shows, the results of the non-rigid ICP algorithm cannot distinguish the AIS subjects and the normal subjects. For example, an AIS subject (left) has $E_H = 14.8$, but, one normal subject

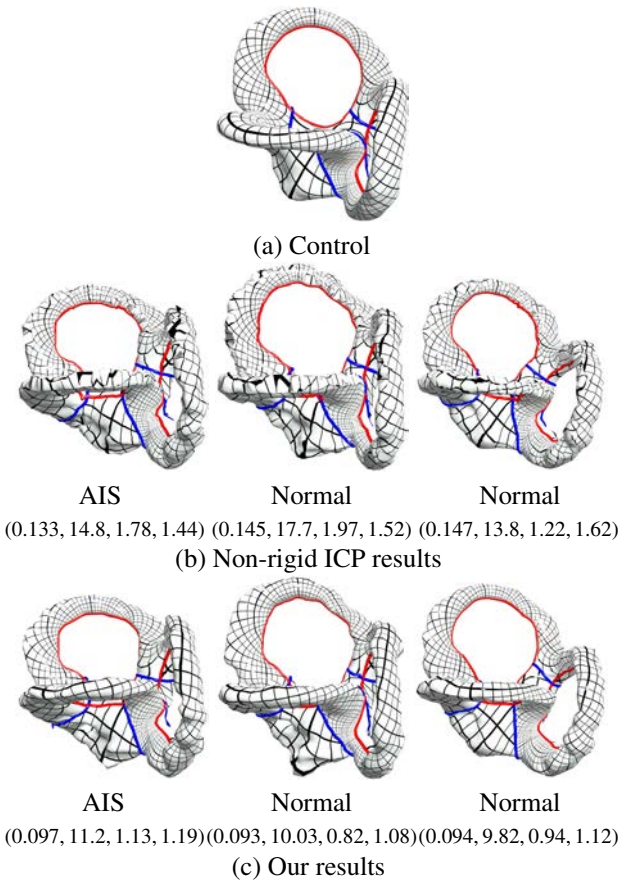

Figure 10: Experimental results. We map the control model M to a VS subject N and then measure various types of geometric difference between M and N. The landmarks can be matched exactly. The 4-tuple under each model shows the measures E_K, E_H, E_C and E_A, respectively. Using our approach, the AIS subjects have consistently larger distortion measures than the normal subjects. However, the results of the non-rigid ICP algorithm are not consistent.

(middle) has $E_H = 17.7$ and the other normal subject (right) has $E_H = 13.8$. Our method, in sharp contrast, is intrinsic and can guarantee that the resulted map is a homeomorphism. We observed that the majority of our results are very stable so that the distortion measures of the AISs are consistently higher than the normal subjects. In particular, using the mean curvature measure E_H, our method can clearly distinguish the AIS subjects and the normal subjects, whereas the non-rigid ICP algorithm fails (see Figure 7 row 2).

Another limitation of the non-rigid ICP algorithm [5] is its high computational cost. In each iteration, the algorithm solves a linear system $\mathbf{A}^T\mathbf{A}\mathbf{X} = \mathbf{A}^T\mathbf{B}$, where $\mathbf{A}$ is of size $(4E+V)\times 4V$ and B of size $(4E+V)\times 3$, V and E are the number of vertices and edges of the target mesh. Experimental results show that the non-rigid ICP algorithm converges in 200 to 300 iterations and each iteration takes 5 seconds on average. Our method computes the harmonic maps and holomorphic 1-forms, which are all based on solving sparse linear systems of size $V \times V$. Thus, our implementation is straightforward and the performance of our method is much better than the non-rigid ICP algorithm.

We should point out that the existing methods aim at solving the registration problem for general 3D surfaces, whereas our application domain is limited to the genus-3 vestibular system, since both our landmark extraction and registration take advantage of the unique geometric as well as topological features of the VS. Our *ad hoc* solution is robust, fully automatic and highly efficient.

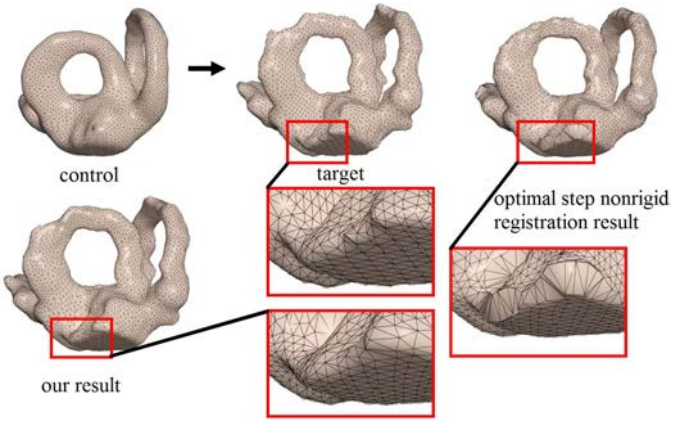

Figure 11: Comparison. The optimal step non-rigid ICP algorithm [7] iteratively deforms the control VS towards the target. The deformation is carried out in an extrinsic manner, which cannot guarantee the bijectivity. Furthermore, since the control VS is very smooth and the target VS has features (see the red close-up view), the template (the control shape) can easily stuck into a local optimal, which produces large distortion. One can clearly see the difference between the target and the result by the non-rigid ICP algorithm. In contrast, our method is completely intrinsic and guarantees the registration is a homeomorphism. All the features on the target are well preserved by our algorithm.

5. Conclusion

This paper presents an effective and practical solution to register the genus-3 vestibular systems. Our method first extracts six geodesic landmarks for the VS, which are stable, intrinsic, and insensitive to the VS's resolution and tessellation. Moreover, they are highly consistent regardless of the disease and normal groups. The detected geodesic landmarks partition the VS into three patches, a topological annulus and two topological disks. For each pair of patches of the AIS subject and the control, we compute a bijective map using the holomorphic 1-form and harmonic map techniques. With a carefully designed boundary condition, the three individual maps can be glued in a seamless manner so that the resulting registration is a homeomorphism with exact landmark matching. Our method is robust, efficient and fully automatic. It takes only a few seconds on a PC, which significantly outperforms the non-rigid ICP algorithm. We conducted a student's t-test on the test data. Computational results show that using the mean curvature measure E_H, our method can clearly distinguish the AIS subjects and the normal subjects.

Acknowledgement

This project was partially supported by Singapore Ministry of Education (MOE) grants RG40/12 and MOE2013-T2-2-011, China NSF grants No. 61170170 and No. 61271366, and the Capital Science and Technology Platform project No. Z131110000613062. We thank the anonymous reviewers for their valuable comments.

References

[1] N. N. Byl, J. M. Gray, Complex balance reactions in different sensory conditions: adolescents with and without idiopathic scoliosis, Journal of Orthopaedic Research 11(2) (1993) 215–227. 2

[2] M. Simoneau, V. Lamothe, E. Hutin, P. Mercier, N. Teasdale, J. Blouin, Evidence for cognitive vestibular integration impairment in idiopathic scoliosis patients, BMC Neuroscience 10 (1) (2009) 1–7. 2

[3] W. Zeng, L. M. Lui, L. Shi, D. Wang, W. C. Chu, J. C. Cheng, J. Hua, S.-T. Yau, X. Gu, Shape analysis of vestibular systems in adolescent idiopathic scoliosis using geodesic spectra, in: Medical Image Computing and Computer-Assisted Intervention MICCAI 2010, Vol. 6363 of Lecture Notes in Computer Science, 2010, pp. 538–546. 2

[4] S.-Q. Xin, Y. He, C.-W. Fu, D. Wang, S. Lin, W. C. Chu, J. C. Cheng, X. Gu, L. M. Lui, Euclidean geodesic loops on high-genus surfaces applied to the morphometry of vestibular systems, in: Proceedings of MICCAI '11: Part II, 2011, pp. 384–392. 2, 4

[5] P. J. Besl, N. D. McKay, A method for registration of 3-d shapes, IEEE Trans. Pattern Anal. Mach. Intell. 14 (2) (1992) 239–256. 3, 7, 8, 9

[6] Q.-X. Huang, B. Adams, M. Wicke, L. J. Guibas, Non-rigid registration under isometric deformations, in: Proceedings of the Symposium on Geometry Processing, SGP '08, 2008, pp. 1449–1457. 3, 4

[7] B. Amberg, S. Romdhani, T. Vetter, Optimal step nonrigid icp algorithms for surface registration, in: Computer Vision and Pattern Recognition, 2007. CVPR '07. IEEE Conference on, 2007, pp. 1–8. 3, 4, 8, 9

[8] M. Salzmann, F. Moreno-Noguer, V. Lepetit, P. Fua, Closed-form solution to non-rigid 3d surface registration, in: Computer Vision ECCV 2008, Vol. 5305 of Lecture Notes in Computer Science, 2008, pp. 581–594. 3, 4

[9] M. F. Beg, M. I. Miller, A. Trouve, L. Younes, Computing large deformation metric mappings via geodesic flows of diffeomorphisms, International Journal of Computer Vision 61(2) (2005) 139–157. 3, 4, 7

[10] S. C. Joshi, M. I. Miller, Landmark matching via large deformation diffeomorphisms, IEEE Transaction on Image Processing 9 (8) (2000) 1357–1370. 3

[11] A. Qiu, L. Youne, M. I. Miller, Principal component based diffeomorphic surface mapping, IEEE Transactions on Medical Imaging 31 (2) (2012) 302–311. 3

[12] X. Gu, Y. Wang, T. F. Chan, P. M. Thompson, S.-T. Yau, Genus zero surface conformal mapping and its application to brain surface mapping, IEEE Transactions on Medical Imaging 23 (8) (2004) 949–958. 3

[13] Y. Wang, L. M. Lui, T. F. Chan, P. M. Thompson, Optimization of brain conformal mapping with landmarks, in: Proceedings of MICCAI '05: Part II, 2005, pp. 675–683. 3

[14] W. Zeng, Y. Zeng, Y. Wang, X. Yin, X. Gu, D. Samaras, 3d non-rigid surface matching and registration based on holomorphic differentials, in: Computer Vision ECCV 2008, Vol. 5304 of Lecture Notes in Computer Science, 2008, pp. 1–14. 3, 4

[15] W. Zeng, F. Luo, S.-T. Yau, X. Gu, Surface quasi-conformal mapping by solving beltrami equations, in: Mathematics of Surfaces XIII, Vol. 5654 of Lecture Notes in Computer Science, 2009, pp. 391–408. 3

[16] L. M. Lui, T. W. Wong, P. Thompson, T. Chan, X. Gu, S.-T. Yau, Shape-based diffeomorphic registration on hippocampal surfaces using beltrami holomorphic flow, in: Proceedings of MICCAI '10: Part II., 2010, pp. 323–330. 3

[17] L. M. Lui, K. C. Lam, S.-T. Yau, X. Gu, Teichmuller mapping (t-map) and its applications to landmark matching registrations, arXiv:1211.2569 (2012). 3, 4

[18] O. Weber, A. Myles, D. Zorin, Computing extremal quasiconformal maps, Comp. Graph. Forum 31 (5) (2012) 1679–1689. 3

[19] T. K. Dey, K. Li, J. Sun, D. Cohen-Steiner, Computing geometry-aware handle and tunnel loops in 3d models, ACM Transactions on Graphics 27 (3) (2008) 45:1–45:9. 4

[20] S.-Q. Xin, Y. He, C.-W. Fu, Efficiently computing exact geodesic loops within finite steps, IEEE Transactions on Visualization and Computer Graphics 18 (6) (2012) 879–889. 4, 5

[21] X. Gu, S.-T. Yau, Global conformal surface parameterization, in: Proceedings of the 2003 Eurographics/ACM SIGGRAPH Symposium on Geometry Processing, 2003, pp. 127–137. 5

[22] M. Miller, A. Trouve, L. Younes, On the metrics and euler-lagrange equations of computational anatomy, Annual Review of Biomedical Engineering 4 (2002) 375–405. 7